FOSSEE, IIT Bombay
OpenFOAM Research Migration Project
May 2026

FOSSEE CFD-OpenFOAM Semester Long Internship Spring 2026

on

CFD Analysis of Free-Falling Disks Using Overset Mesh Techniques

Duruseti Srija[1], Nikhil Chitnavis[2], and Chandan Bose[3]

[1]Department of Mechanical Engineering, Indian Institute of Technology Kanpur, Kanpur, India
[2]Ph.D. Research Scholar, Indian Institute of Technology Madras, Chennai, India
[3]Assistant Professor, Department of Aerospace Engineering, University of Birmingham, Birmingham, United Kingdom

June 23, 2026

Synopsis

This study presented a numerical investigation of freely falling solid and annular disks using overset mesh techniques in OpenFOAM. Three-dimensional transient simulations were performed under laminar flow conditions using six-degree-of-freedom (6-DoF) rigid-body motion. The study focused on the influence of body geometry on downstream flow behavior during steady free fall in the low Reynolds number regime. Comparisons between the solid and annular disks showed that the central opening in the annular geometry modified the downstream flow structure and streamline distribution. The results demonstrated the capability of overset mesh methods for moving-body simulations involving freely falling bluff bodies.

Keywords: OpenFOAM, Overset Mesh, Free-Falling Disk, Annular Disk, 6-DoF Motion, Laminar Flow, Bluff Body Aerodynamics

1 Introduction

The study of freely falling bodies in fluid media is an important area of fluid mechanics due to its relevance in several engineering and physical applications such as particulate transport, sedimentation, aerosol motion, underwater systems, and bluff-body aerodynamics. When a body falls through a fluid under the influence of gravity, the surrounding flow interacts continuously with the moving surface of the body, producing complex pressure distributions, flow separation, and downstream recirculation regions. The resulting flow characteristics depend strongly on parameters such as body geometry, Reynolds number, fluid properties, and body motion.

Disks are commonly used as canonical bluff-body configurations for studying separated flows because of their simple geometry and well-defined wake structures. During free fall, the sharp edges of a disk cause boundary layer separation, generating downstream recirculation zones and organized wake structures behind the body. Depending on the Reynolds number, freely falling disks may exhibit different motion regimes such as steady falling, oscillatory motion, fluttering, tumbling, and chaotic trajectories. In the low Reynolds number regime considered in this study, the motion remains predominantly stable and corresponds to steady free fall.

In addition to conventional solid disks, annular disks represent an important modified bluff-body geometry. Unlike a solid disk, an annular disk contains a central opening that allows partial penetration of fluid through the body during motion. This geometric modification alters the pressure distribution and downstream wake organization compared to a solid disk of similar dimensions. The interaction between the outer separated flow and the fluid passing through the annular opening modifies the downstream recirculation behavior and overall flow development.

Numerical simulation of freely falling bodies presents significant challenges because the body continuously moves through the computational domain. Conventional mesh deformation techniques often lead to severe mesh distortion and deterioration of mesh quality during large body displacements.

To overcome these limitations, the present study employs the overset mesh technique, also known as the Chimera mesh method. In this approach, separate meshes are generated for the moving body region and the stationary background domain. The moving overset mesh surrounding the body overlaps with the background mesh, and flow information is exchanged between the overlapping regions through interpolation.

The simulations were carried out using OpenFOAM. The `overPimpleDyMFoam` solver was employed for solving the incompressible transient flow equations together with dynamic overset mesh motion. The motion of the disks was modeled using six-degree-of-freedom (6-DoF) rigid-body dynamics, allowing the bodies to respond naturally to gravitational and hydrodynamic forces during free fall.

2 Problem Definition

To numerically investigate the steady free-fall motion of solid and annular disks using overset mesh techniques in OpenFOAM and examine the influence of disk geometry on wake formation and downstream recirculation under laminar flow conditions.

3 Governing Equations and Numerical Methodology

The flow was modeled as incompressible, transient, and laminar. The `overPimpleDyMFoam` solver was employed to solve the continuity and Navier–Stokes equations on an overset mesh system while coupling the fluid flow with six-degree-of-freedom (6-DoF) rigid-body motion.

3.1 Continuity Equation

$$\nabla \cdot \mathbf{U} = 0$$

Equation (1) represents conservation of mass for incompressible flow, requiring the velocity field to remain divergence-free throughout the simulation.

3.2 Momentum Equation

$$\frac{\partial \mathbf{U}}{\partial t} + (\mathbf{U} \cdot \nabla)\mathbf{U} = -\frac{1}{\rho}\nabla p + \nu \nabla^2 \mathbf{U} + \mathbf{g}$$

where:

- $\mathbf{U}$ – velocity vector,
- p – pressure,
- ρ – fluid density,
- ν – kinematic viscosity,
- $\mathbf{g}$ – gravitational acceleration.

3.3 Rigid-Body Motion (6-DoF)

The motion of the freely falling body is governed by Newton's second law:

$$m\frac{d\mathbf{v}}{dt} = \mathbf{F}_{\text{fluid}} + m\mathbf{g}$$

$$\mathbf{I}\frac{d\boldsymbol{\omega}}{dt} + \boldsymbol{\omega} \times (\mathbf{I}\boldsymbol{\omega}) = \mathbf{M}_{\text{fluid}}$$

where $\mathbf{v}$ and $\boldsymbol{\omega}$ represent the linear and angular velocities, while $\mathbf{F}_{\text{fluid}}$ and $\mathbf{M}_{\text{fluid}}$ denote the hydrodynamic force and moment acting on the body.

3.4 Effective Mass and Moment of Inertia

The effective mass of the freely falling body is given by

$$m_{\text{eff}} = (\rho_s - \rho_l)V$$

where ρ_s is the solid density, ρ_l is the fluid density, and V is the body volume.
The body mass used for moment of inertia calculations is

$$m = \rho_s V$$

For the solid disk geometry, the principal moments of inertia are

$$I_{xx} = I_{yy} = \frac{1}{12} m(3R^2 + t^2)$$

$$I_{zz} = \frac{1}{2} mR^2$$

where R is the disk radius and t is the disk thickness.
For the annular disk geometry, the moments of inertia are

$$I_{xx} = I_{yy} = \frac{1}{12} m\left[3(R_o^2 + R_i^2) + t^2\right]$$

$$I_{zz} = \frac{1}{2} m(R_o^2 + R_i^2)$$

where R_o and R_i denote the outer and inner radii of the annular disk, respectively.

4 Geometry and Mesh

4.1 Geometry and Computational Domain

The computational domain was developed to simulate the gravity-driven free-fall motion of solid and annular disks using the overset mesh framework available in OpenFOAM. The domain consisted of a stationary background region together with a moving overset region surrounding the freely falling body.

A rectangular background domain of dimensions 10 cm $\times$ 10 cm $\times$ 16 cm was used to provide sufficient space for wake development during free fall. The overall computational setup, including the background domain, overset region, and freely falling disk geometry, is illustrated in Figure 1.

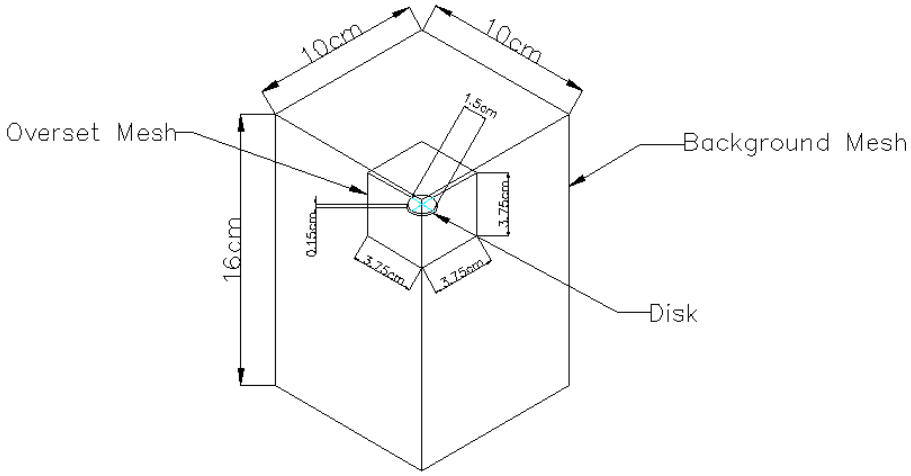

Figure 1: Schematic representation of the computational domain showing the background mesh region, moving overset mesh region, and freely falling disk geometry.

The structured background mesh used for the stationary region is shown in Figure 2.

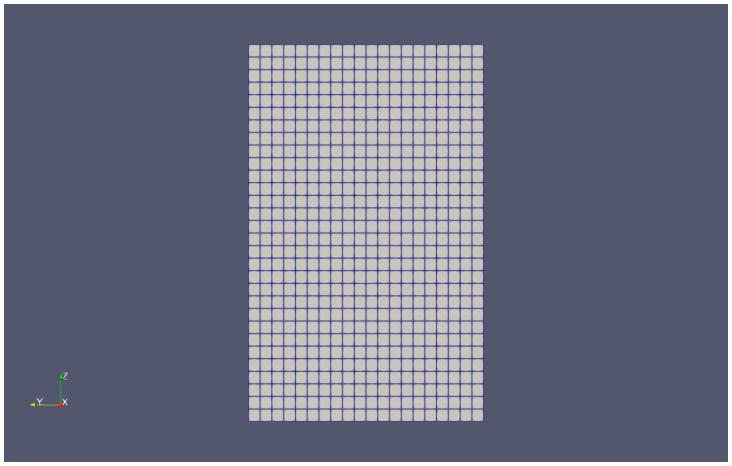

Figure 2: Structured background mesh used for the stationary computational domain.

Two disk geometries were investigated: a solid disk and an annular disk containing a concentric central opening. The annular geometry allowed partial flow penetration through the body and modified the downstream wake structure relative to the solid disk configuration.

The freely falling body was enclosed inside a moving overset mesh region to allow rigid-body motion without mesh deformation. The overset mesh overlapped with the stationary background mesh, enabling interpolation of flow variables between the two regions during motion.

The principal geometrical dimensions used in the simulations are summarized in Table 1.

Table 1: Geometrical dimensions used in the simulations

Parameter	Dimension
Background domain length	10 cm
Background domain width	10 cm
Background domain height	16 cm
Disk outer diameter	1.5 cm
Annular disk inner diameter	0.75 cm
Disk thickness	1.5 mm
Overset region size	3.75 cm

4.2 Mesh Configuration

A structured Cartesian mesh was generated for the background region, while body-fitted overset meshes surrounding the disks were generated using the `snappyHexMesh` utility. Local refinement was introduced near the freely falling body to improve the resolution of near-body flow structures and overset interpolation.

The mesh generation procedure involved:

- generation of the structured background mesh using `blockMesh`,
- creation of body-fitted overset meshes using `snappyHexMesh`,
- local refinement near the disk surface,
- and merging of the overset and stationary mesh regions.

Figure 3 shows the locally refined overset meshes used for the solid and annular disk configurations.

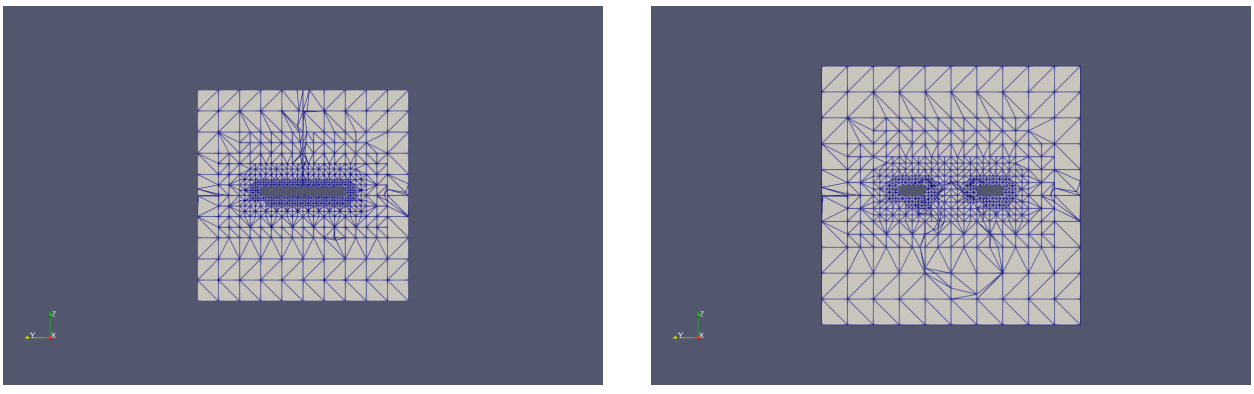

Figure 3: Locally refined overset mesh surrounding the solid disk (left) and annular disk (right).

Mesh refinement was applied near the body surface and wake-development region to improve the spatial resolution of the transient flow structures while maintaining a comparatively coarser mesh away from the body to reduce computational cost.

The overset interpolation regions used during mesh motion are illustrated in Figure 4.

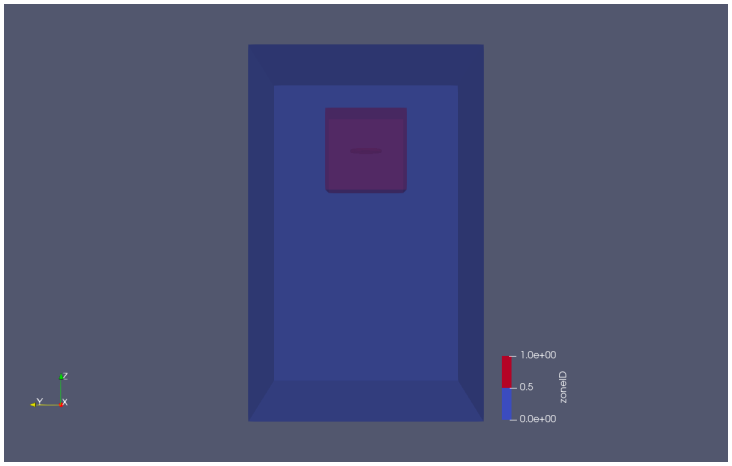

Figure 4: Zone identification used for overset interpolation between the stationary and moving mesh regions.

The final merged mesh configurations used for the solid and annular disk simulations are shown in Figure 5.

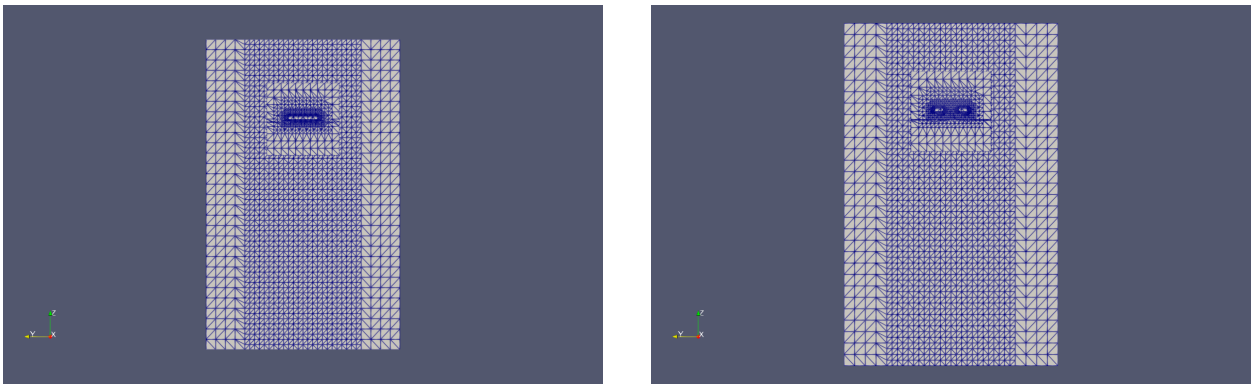

Figure 5: Final merged mesh configuration for the solid disk case (left) and annular disk case (right).

The overset mesh methodology enabled independent rigid-body motion of the disks while preserving mesh quality throughout the transient simulations.

5 Boundary Conditions

The boundary conditions used for the pressure field (`p`), velocity field (`U`), and mesh motion field (`pointDisplacement`) are summarized in the following tables.

5.1 Pressure Boundary Conditions

Table 2: Pressure boundary conditions

Boundary	Condition
Inlet	zeroGradient
Outlet	zeroGradient
Top	zeroGradient
Bottom	zeroGradient
Disk Surface	zeroGradient
Front and Back	fixedValue
Overset Interface	overset

A zero-gradient condition was applied to most pressure boundaries to allow the pressure field to adjust naturally during transient free-fall motion. The front-and-back boundaries were assigned fixed pressure values, while the overset interface employed the `overset` condition for interpolation between overlapping mesh regions.

5.2 Velocity Boundary Conditions

Table 3: Velocity boundary conditions

Boundary	Condition
Inlet	fixedValue (0 0 0)
Outlet	fixedValue (0 0 0)
Top	fixedValue (0 0 0)
Bottom	fixedValue (0 0 0)
Front and Back	fixedValue (0 0 0)
Disk Surface	movingWallVelocity
Overset Interface	overset

Fixed-value zero-velocity conditions were applied at the stationary boundaries. The disk surface employed the `movingWallVelocity` condition to account for rigid-body motion obtained from the six-degree-of-freedom solver. Velocity interpolation between the moving overset mesh and stationary background mesh was handled using the `overset` condition.

5.3 Point Displacement Boundary Conditions

Table 4: Point displacement boundary conditions

Boundary	Condition
Overset Interface	zeroGradient
Disk Surface	calculated
Remaining Boundaries	fixedValue (0 0 0)

The `pointDisplacement` field was used to control mesh motion within the overset framework. Stationary boundaries were assigned zero displacement, while disk motion was calculated automatically from the rigid-body motion solver.

6 Solver Setup

6.1 overPimpleDyMFoam Solver

The simulations were performed using the `overPimpleDyMFoam` solver available in OpenFOAM. This solver is designed for transient incompressible flow simulations involving dynamic mesh motion and overset mesh techniques. The solver combines the pressure–velocity coupling of the PIMPLE algorithm with dynamic overset mesh handling.

The PIMPLE algorithm combines the features of the PISO and SIMPLE methods to provide stable transient simulations while maintaining accurate pressure–velocity coupling.

During each time step, the solver performs the following operations:

1. Update overset mesh connectivity and moving mesh regions.
2. Solve the momentum equation to obtain the predicted velocity field.
3. Solve the pressure equation and correct the velocity field to satisfy continuity.
4. Perform PIMPLE correction iterations for pressure–velocity coupling.
5. Compute hydrodynamic forces and moments acting on the body surface.
6. Update the six-degree-of-freedom rigid-body motion using gravitational and hydrodynamic forces.
7. Move the overset mesh according to the updated body position.

The overset mesh methodology enabled large body displacements without mesh deformation while maintaining interpolation between the stationary background mesh and moving body mesh.

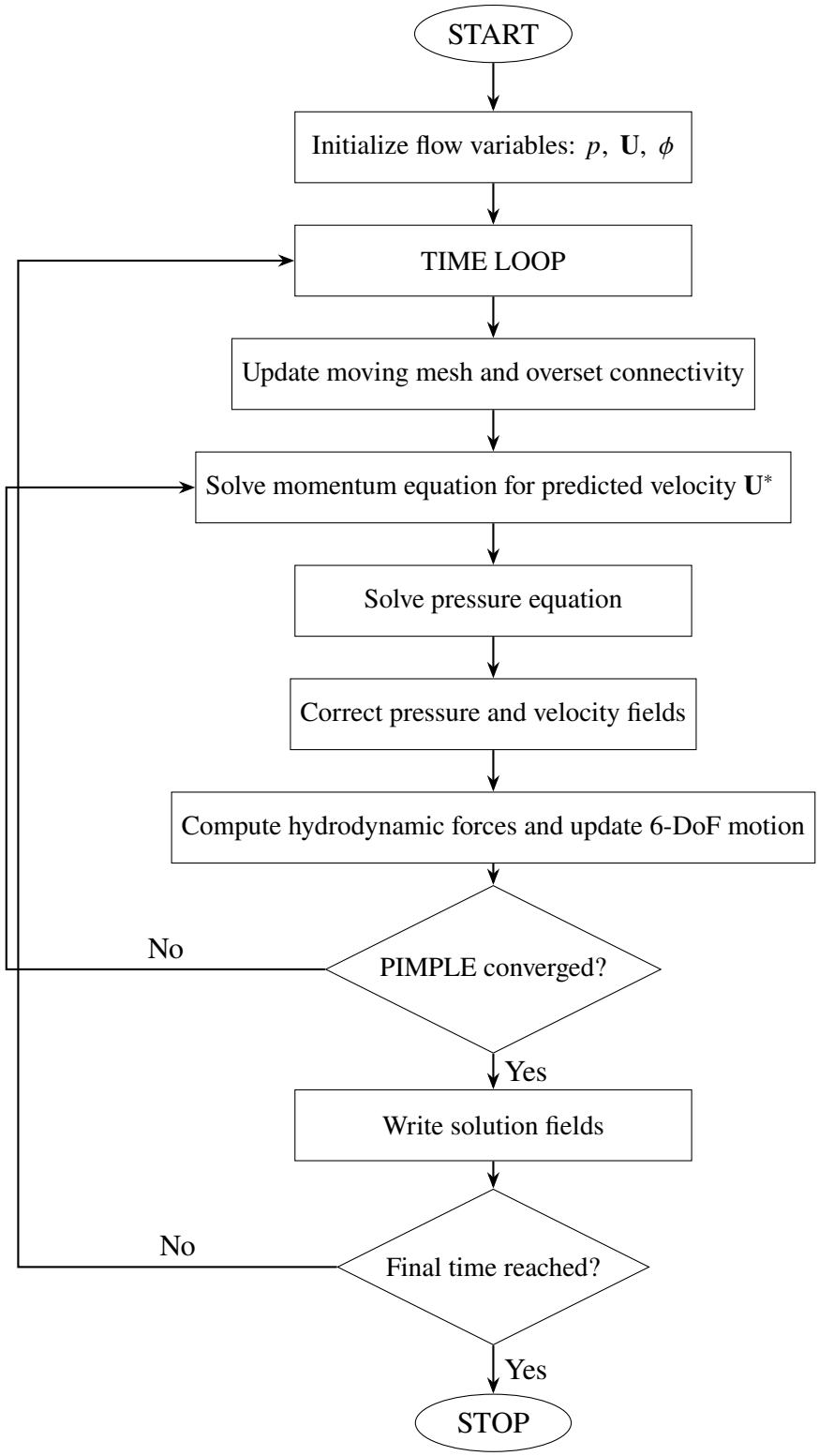

Figure 6: Flowchart of the `overPimpleDyMFoam` solver algorithm

6.2 Fluid Properties

The fluid was modeled as an incompressible Newtonian fluid with constant density and viscosity throughout the computational domain. The fluid properties specified in the `transportProperties` dictionary are summarized in Table 5.

Table 5: Fluid properties used in the simulations

Parameter	Value	Description
Transport model	Newtonian	Incompressible Newtonian fluid
ν	3.85×10^{-4} m^2/s	Kinematic viscosity
ρ	970 kg/m^3	Fluid density

The selected fluid properties correspond to a viscous liquid medium suitable for freely falling bluff-body simulations in the low Reynolds number regime.

6.3 6-DoF Motion Properties

The rigid-body motion of the freely falling disks was modeled using the `sixDoFRigidBodyMotion` solver coupled with the dynamic overset mesh framework. The principal motion properties used in the simulations are summarized in Table 6.

Table 6: 6-DoF motion properties used in the simulations

Parameter	Value	Description
Motion solver	`sixDoFRigidBodyMotion`	Rigid-body motion solver
Dynamic mesh type	`dynamicOversetFvMesh`	Overset mesh motion handling
Moving patch	`disk`	Freely falling body surface
Effective mass	4×10^{-4} kg	Effective body mass
Centre of mass	$(0, 0, 0.00075)$	Body center location
Fluid density	970 kg/m^3	Reference fluid density
Gravity vector	$(0, 0, -9.81)$	Gravitational acceleration
Acceleration relaxation	0.4	Motion stabilization parameter
Acceleration damping	0.4	Numerical damping parameter
Time integration scheme	Newmark	Time integration method

The body motion was driven by gravitational acceleration and hydrodynamic forces obtained from the transient flow solution. The Newmark integration scheme was used for temporal integration of the rigid-body equations of motion.

Solid Disk

The solid disk geometry had a radius of 7.5×10^{-3} m and thickness of 1.5×10^{-3} m. The principal moments of inertia were calculated as

$$I_{xx} = I_{yy} = \frac{1}{12} m(3R^2 + t^2)$$

$$I_{zz} = \frac{1}{2} mR^2$$

resulting in

$$I_{xx} = I_{yy} = 9.37 \times 10^{-9} \text{ kg m}^2$$

$$I_{zz} = 1.85 \times 10^{-8} \text{ kg m}^2$$

Annular Disk

The annular disk geometry had an outer radius of 7.5×10^{-3} m, inner radius of 3.75×10^{-3} m, and thickness of 1.5×10^{-3} m.

The principal moments of inertia were calculated as

$$I_{xx} = I_{yy} = \frac{1}{12} m \left[3(R_o^2 + R_i^2) + t^2\right]$$

$$I_{zz} = \frac{1}{2} m(R_o^2 + R_i^2)$$

resulting in

$$I_{xx} = I_{yy} = 1.07 \times 10^{-8} \text{ kg m}^2$$

$$I_{zz} = 2.09 \times 10^{-8} \text{ kg m}^2$$

The calculated inertia values were specified in the `motionProperties` dictionary to ensure physically consistent rotational behavior during the free-fall simulations.

6.4 Numerical Schemes and Solver Settings

The simulations were performed using the finite-volume framework in OpenFOAM v2512. Temporal discretization was performed using the first-order implicit Euler scheme to ensure stable transient integration during overset mesh motion:

```
ddtSchemes
{
    default Euler;
}
```

Spatial convection terms were discretized using bounded limited-linear schemes:

```
div(phi,U)      Gauss limitedLinearV 1;
```

Diffusion terms were discretized using the corrected Gauss linear scheme:

```
laplacianSchemes
{
    default Gauss linear corrected;
}
```

Overset interpolation between the stationary background mesh and moving body mesh was performed using the inverse-distance interpolation method:

```
oversetInterpolation
{
    method          inverseDistance;
}
```

Pressure–velocity coupling was handled using the PIMPLE algorithm:

```
PIMPLE
{
    momentumPredictor   no;

    nOuterCorrectors    10;
    nCorrectors         1;

    moveMeshOuterCorrectors yes;
}
```

The pressure equation was solved using the PBiCGStab solver with DILU preconditioning, while the velocity equation was solved using the smoothSolver with the symGaussSeidel smoother:

```
p
{
    solver          PBiCGStab;
    preconditioner  DILU;
}

U
{
    solver          smoothSolver;
    smoother        symGaussSeidel;
}
```

These solver settings provided stable convergence behavior throughout the transient free-fall simulations.

7 Results and Discussions

7.1 Flow Field Visualization

7.1.1 Velocity Contours

For the solid disk, the velocity contours show the formation of a larger wake region downstream of the body. The disturbed flow extends further into the computational domain, with high velocity gradients near the disk edges.

For the annular disk, the contours show flow penetration through the central opening. The wake region remains comparatively narrower and more confined near the body. Two localized low-velocity regions are visible near the annular opening.

At later time ($t = 1.00$ s), the wake region increases for both geometries. However, the solid disk continues to exhibit a broader downstream disturbed region compared to the annular disk.

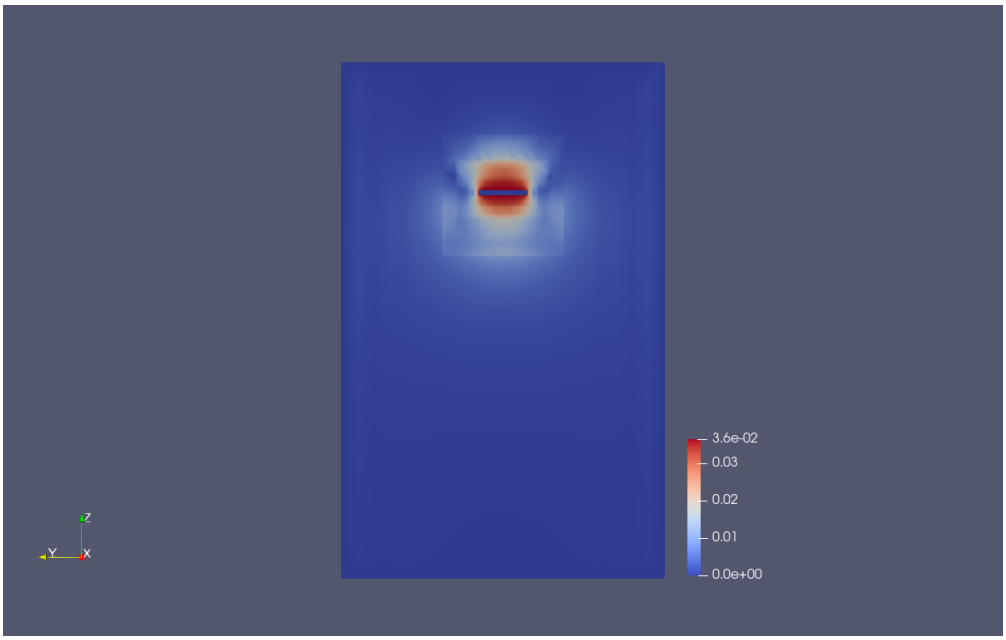

Figure 7: Velocity contours around the solid disk at $t = 0.05$ s.

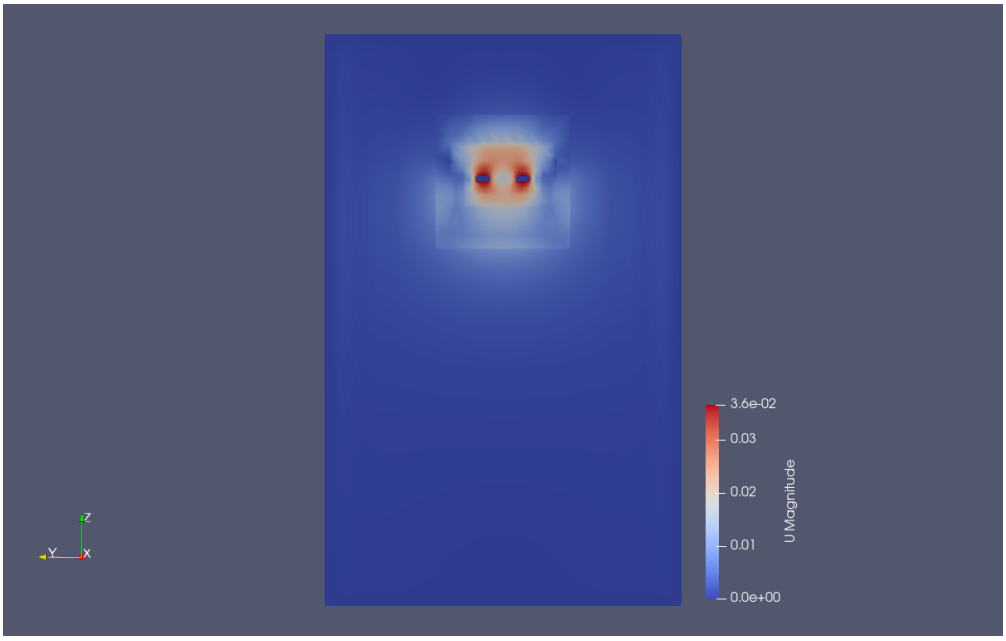

Figure 8: Velocity contours around the annular disk at $t = 0.05$ s.

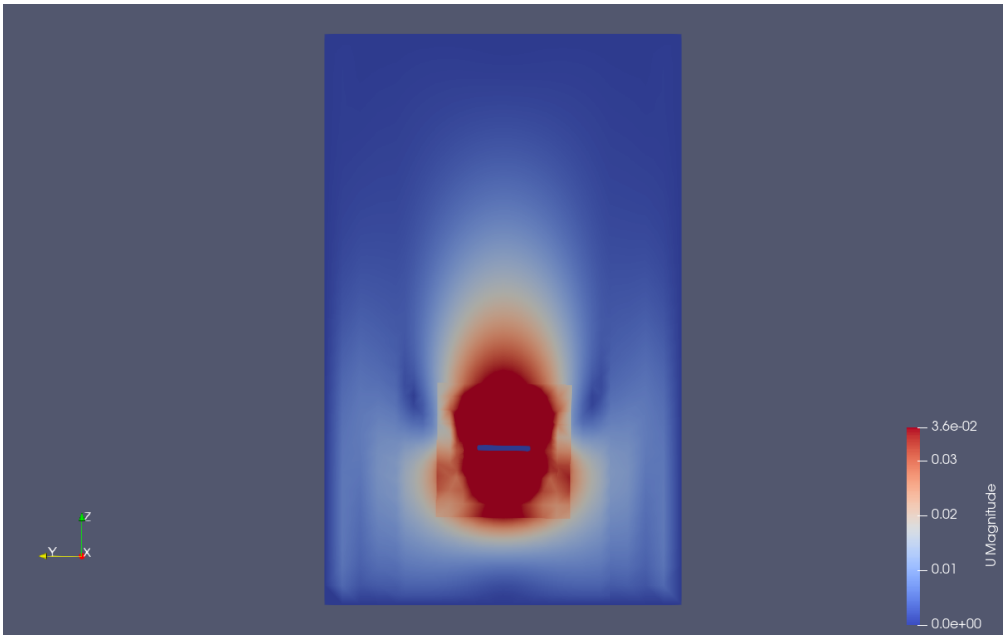

Figure 9: Velocity contours around the solid disk at $t = 1.00$ s.

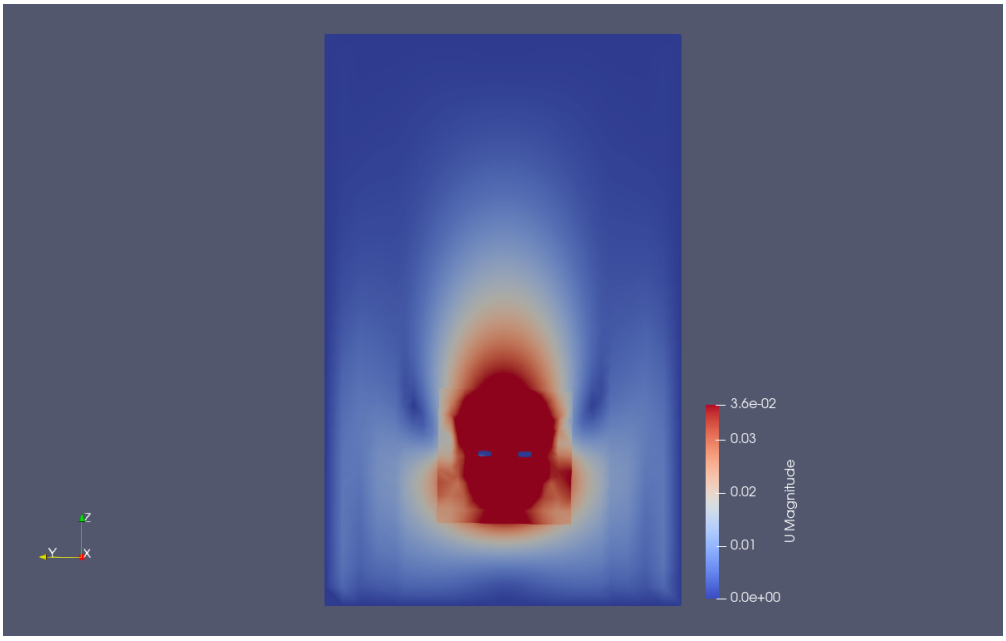

Figure 10: Velocity contours around the annular disk at $t = 1.00$ s.

7.1.2 Streamline Analysis

Figure 11 and Figure 12 present the streamline patterns around the solid and annular disks during free-fall motion.

At $t = 0.05$ s, recirculating streamline structures are observed around both disk configurations. The solid disk exhibits comparatively larger recirculation loops extending farther away from the body surface. For the annular disk, the streamline structures remain more confined near the disk, and flow development is modified by the presence of the central opening.

At $t = 1.25$ s, the wake structures become more developed for both geometries. The solid disk continues to exhibit broader downstream recirculation regions, while the annular disk shows comparatively narrower streamline distributions around the wake region. The flow field near the annular disk is influenced by fluid motion through the central opening, producing modified streamline trajectories relative to the solid disk configuration.

The streamline visualizations indicate that the introduction of the central hole alters the wake structure and downstream flow development during free-fall motion.

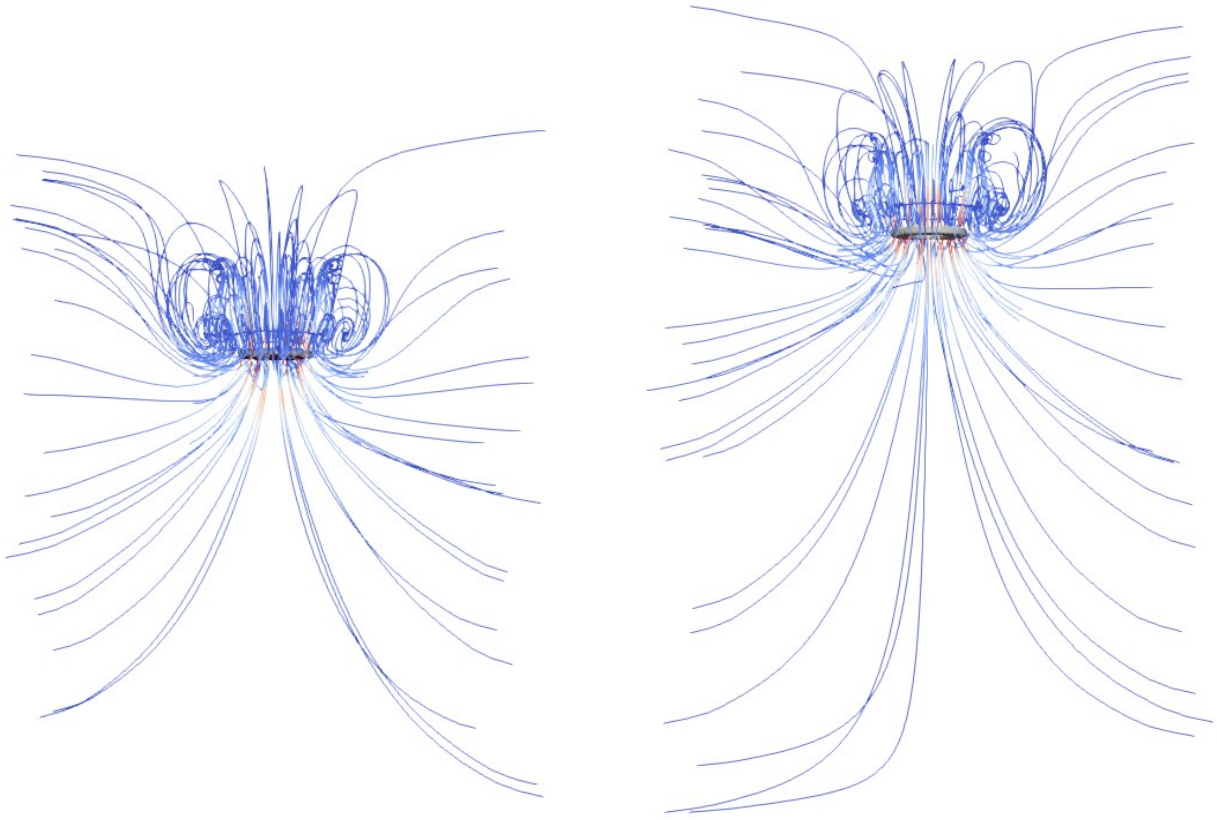

Figure 11: Streamline distribution for the solid disk (left) and annular disk (right) at $t = 0.05$ s.

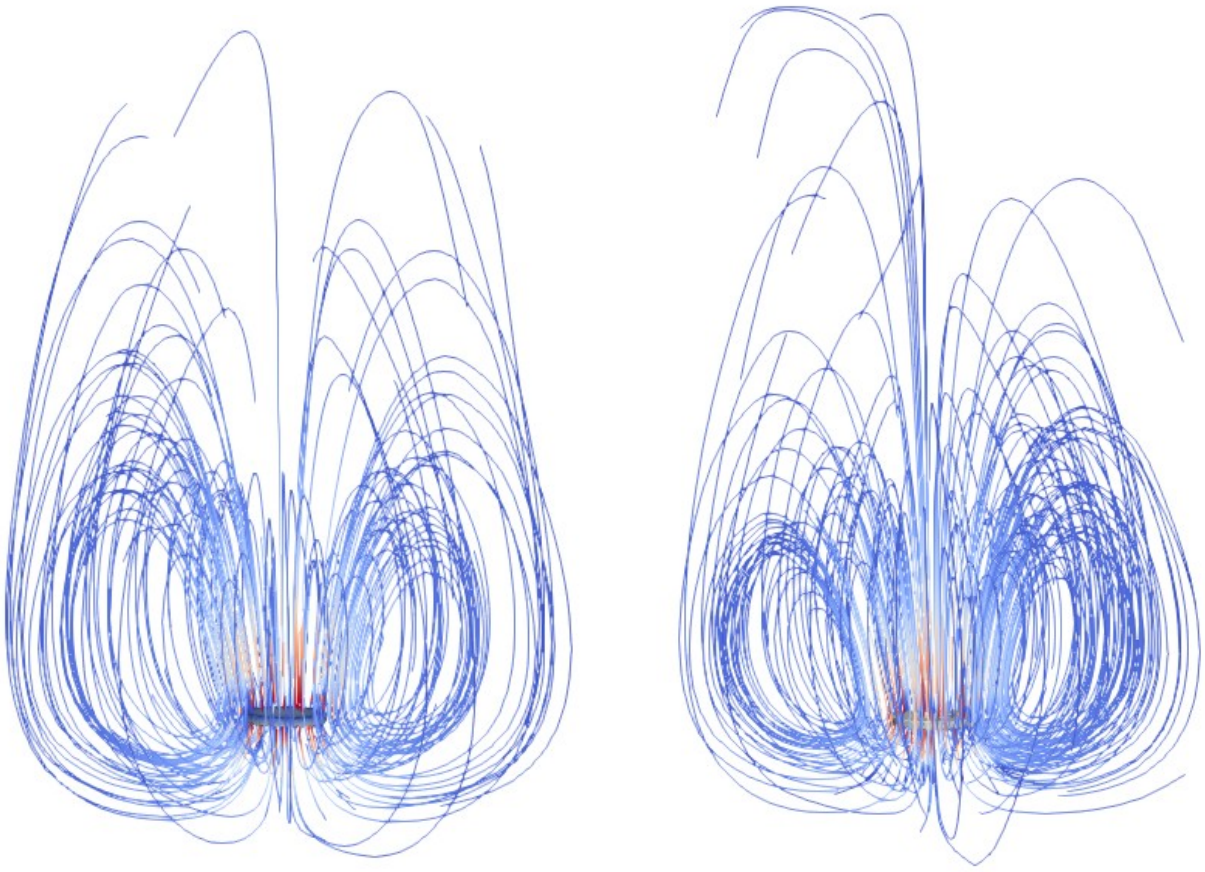

Figure 12: Streamline distribution for the solid disk (left) and annular disk (right) at $t = 1.25$ s.

8 Conclusions

The present study investigated the free-fall behavior of solid and annular disks using an overset mesh approach in OpenFOAM. Velocity contours and streamline visualizations were analyzed to examine the influence of the central opening on the surrounding flow field.

The simulations showed noticeable differences in the wake structure between the solid and annular disk configurations. The solid disk produced comparatively broader recirculation regions and larger streamline loops in the downstream wake. In contrast, the annular disk exhibited more confined wake structures, with the flow field influenced by fluid motion through the central opening.

The streamline and velocity contour visualizations demonstrated that the introduction of a central hole modifies the downstream flow development around the falling body. The overset mesh methodology successfully captured the transient motion of the freely falling disks while maintaining mesh quality during body motion.

Overall, the numerical results qualitatively reproduced the flow-field modifications associated with annular disk geometries reported in previous experimental studies on freely falling disks.

9 Acknowledgement

I would like to sincerely thank Prof. Chandan Bose, my project guide, for his continuous support, encouragement, and guidance throughout the internship. His mentorship and enthusiasm toward Computational Fluid Dynamics motivated me to further explore this field and develop a deeper interest in OpenFOAM-based simulations. The resources, tutorials, and discussions provided during the internship greatly contributed to my learning experience.

I would also like to express my heartfelt gratitude to Ms. Payel Mukherjee, Project Manager of the CFD OpenFOAM Team at FOSSEE, for her constant support and assistance throughout the internship. She patiently addressed my queries and created a welcoming and encouraging learning environment. Her guidance made the internship experience both comfortable and motivating.

References

[1] OpenFOAM Foundation, *OpenFOAM User Guide*, Available: `https://www.openfoam.com/documentation`

[2] L. Vincent, W. S. Shambaugh, and E. Kanso, ‘‘Holes stabilize freely falling coins,’’ *Journal of Fluid Mechanics*, vol. 801, pp. 250–259, 2016.

[3] W. Zhang, D. Bi, and Y. Wei, ‘‘Falling styles of perforated disks,’’ *International Journal of Multiphase Flow*, vol. 161, p. 104401, 2023.